JOURNAL OF AIRCRAFT
Vol. 34, No. 6, November–December 1997

High-Performance Supersonic Missile Inlet Design Using Automated Optimization

Ge-Cheng Zha,* Donald Smith,† Mark Schwabacher,‡ Khaled Rasheed,‡ Andrew Gelsey,§ and Doyle Knight¶
Rutgers University, Piscataway, New Jersey 08855-0909
and
Martin Haas**
United Technologies Research Center, East Hartford, Connecticut 06180

A multilevel design strategy for supersonic missile inlet design is developed. The multilevel design strategy combines an efficient simple physical model analysis tool and a sophisticated computational fluid dynamics (CFD) Navier–Stokes analysis tool. The efficient simple analysis tool is incorporated into the optimization loop, and the sophisticated CFD analysis tool is used to verify, select, and filter the final design. The genetic algorithms and multistart gradient line search optimizers are used to search the nonsmooth design space. A geometry model for the supersonic missile inlet is developed. A supersonic missile inlet that starts at Mach 2.6 and cruises at Mach 4 was designed. Significant improvement of the inlet total pressure recovery has been obtained. Detailed flowfield analysis is also presented.

I. Introduction

WITH the advent of powerful computers, aerodynamic design with automated optimization has become increasingly popular with the motivation to achieve a better quality design. The aim of our current work is to develop a technology for supersonic missile aerodynamic design with automated optimization including component performance optimization and mission analysis, etc. The purpose of this paper is to present the study conducted to optimize a supersonic inlet design. This is the first step of the long-term goal. The total pressure recovery coefficient, which represents the aerodynamic performance of the inlet, was chosen as the optimization objective. The external cowl shape and diameter were held constant, and hence, the external cowl wave drag remained fixed for this study.

The missile inlet in this design work is a fixed geometry axisymmetric mixed compression inlet with a cruise Mach number of 4 at 18.3 km (60,000 ft) altitude. To minimize inlet manufacturing cost, expensive performance improvement techniques such as boundary-layer bleed and variable geometry were not considered.

The performance of a supersonic missile inlet depends on many factors such as the extent of external and internal compression, total contraction ratio, inlet start throat area, throat location, shock train length, divergence of subsonic diffuser, etc. The conventional design of such complex aerodynamic systems mainly depends on the experience of the designers who may find it difficult to take into account all of the factors needed to achieve an optimum design. A computer-aided automated optimization technique is therefore very useful.

The optimization technique may be generally classified into two types: 1) gradient-based and 2) nongradient-based methods. Gradient-based methods usually require that the objective functions and constraints are smooth. Conventional gradient-based methods generally introduce a line search to find the optimum. Gelsey et al.[1] and Shukla et al.[2] used a computational fluid dynamics (CFD) solver with the gradient-based line search optimizer C Code for Feasible Sequential Quadratic Programming (CFSQP) (Ref. 3) to redesign two hypersonic inlets. A similar method has been used for the design of three-dimensional wings with nacelles[4] for a supersonic transport. However, such approaches usually require a number of flowfield computations proportional to the number of design variables to obtain the gradients. The optimization would be extremely difficult with a large number of design variables because of the limitation of the computer power. An alternative gradient approach based on control theory suggested by Jameson[5] seems promising to overcome this difficulty. This method uses the flowfield governing equations as constraints and introduces the adjoint equations to make the gradient computation independent of the number of design variables. In principle, the true optimum can only be obtained with unlimited design variables. The optimum approach procedure of control theory method is much more efficient than the line search methods. Control theory has been successfully used to design two-dimensional and three-dimensional wings and three-dimensional wing/body junctions.[6] However, the line search method is simpler and the application is more straightforward as long as the geometry can be modeled without using too many design variables.

The advantage of the gradient-based method is that it is more efficient than the non-gradient method if the design space is smooth. The disadvantage is that it is more likely to stop at nonglobal local optima. The nongradient-based methods [such as genetic algorithms (GA), simulated annealing (SA), and random probes (RP)] are more capable of treating a design space with discontinuities and approaching the global optimum. Yamamoto and Inoue[7] and Dervieux et al.[8] used GA to optimize the design of airfoils. The disadvantage of the nongradient-

Received April 8, 1996; revision received April 7, 1997; accepted for publication June 24, 1997.

*Research Associate, Department of Mechanical and Aerospace Engineering and Center for Computational Design, P.O. Box 909. Member AIAA.

†Assistant Professor, Computer Science Department and Center for Computational Design, P.O. Box 909. Member AIAA.

‡Ph.D. Candidate, Computer Science Department and Center for Computational Design, P.O. Box 909.

§Assistant Professor, Computer Science Department and Center for Computational Design, P.O. Box 909. E-mail: gelsey@cs.rutgers.edu. Member AIAA.

¶Professor, Department of Mechanical and Aerospace Engineering and Center for Computational Design, P.O. Box 909. Associate Fellow AIAA.

**Senior Research Engineer, Advanced Propulsion and Thermofluid Systems Department. Member AIAA.

based methods is that they are generally more CPU intensive. A good strategy may be to use a nongradient method to get close to the global optimum and then use a gradient method to reach the global optimum. Aly et al.[9] used such a method combining SA and a gradient optimizer for airfoil designs. The optimization is switched to a gradient method from SA when it is near the possible global optimum using a criterion defined by Ogot and Alag.[10]

Supersonic inlet design is a difficult task because of the complex flow physics and CPU requirements. This paper may represent the first attempt to design a supersonic missile inlet with automated optimization. For a typical steady state flowfield computation, e.g., flow past a wing, a single converged computation is required for an evaluation of the objective function. For a supersonic missile inlet, it is different. Because the downstream back pressure is not known a priori, a root search iteration is needed to obtain the back pressure corresponding to inlet critical operation. At the critical operation of the inlet, as the start of the normal shock train is located just downstream of the inlet throat. It is the inlet operating point at which the maximum mass flow rate and total pressure recovery (TPR) can be obtained. It is very time consuming to use a CFD solver for the back pressure search. In particular, when the back pressure is close to the critical value, the shock wave system moves very slowly and a very long execution time is necessary to ensure the stability of the shock wave. In addition, it is not like the wing design for which the pressure forces are of the main interest, and hence, an Euler solver can be used. The TPR depends in part on the viscous losses such as the boundary-layer separation induced by shock wave/turbulent boundary-layer interaction. Thus, a Navier–Stokes solver with turbulence modeling is essential. Using a Digital Equipment Corporation (DEC) Alpha 2100 workstation and General Aerodynamic Simulation Program (GASP) CFD code, it usually requires separate computations extending over one week to complete a back pressure search for a given inlet geometry. Thus, it is too expensive to use a CFD flowfield solver alone as an analysis tool for supersonic inlet design. It would be infeasible because of our current computer power limitation if a line search gradient-based optimization is implemented. The control theory optimization method in principle is possible. But it is not straightforward and more work needs to be done to develop the adjoint equations, taking account of the Navier–Stokes solver and multiple shock discontinuity system inside an inlet geometry.

To develop the technology for supersonic inlet automated design optimization based on the current computation capability, we use the following multilevel design strategy.

II. Multilevel Design Strategy

The multilevel design strategy includes two levels of analysis tools: 1) an efficient, simple physics model analysis and 2) a more sophisticated time-consuming CFD Navier–Stokes analysis. The efficient simple analysis tool is incorporated into the design loop and guides the sophisticated CFD Navier–Stokes solver to verify, select, and filter the final design.

As described in the preceding text, it is infeasible to use a Navier–Stokes solver as the optimization analysis tool for the supersonic missile inlet design. We therefore employed a simple inlet analysis code, the NAWC inlet design and analysis code (NIDA) in the optimization loop. NIDA was developed at United Technologies Research Center (UTRC) as an inlet analysis/design tool.[11] It uses a two-dimensional aerodynamic model employing a method of characteristics for the supersonic flow section upstream of the throat, and empirical one-dimensional correlations downstream of the throat for the region of the terminal shock wave/turbulent boundary-layer interaction and subsonic diffuser. For one evaluation of the objective function, NIDA only needs a few seconds on the DEC Alpha 2100 workstation. NIDA is therefore suitable as an analysis tool in the optimization loop. However, because of the simple aerodynamics model used in NIDA, the accuracy of the NIDA results needs to be verified by a more complete CFD solver. In addition, NIDA provides limited details of the flowfield in the supersonic region only, while a Navier–Stokes computation can give the details of the flowfield throughout the inlet.

We can also use the multilevel design strategy to push the low level optimization to the extreme using very little time. Then we can use the high level analysis tool to optimize fewer but important variables for which the low-level analysis tool cannot take into account. Such work has not been done at this stage, but is the direction for future research.

The CFD solver used in this work is the GASP code from Aerosoft, Inc, which solves the Reynolds-averaged Navier–Stokes equations with Chien's k-ε low Reynolds number correction turbulence model. The inviscid terms are evaluated using Roe's scheme, and the viscous fluxes and source terms are represented by central differences.

III. Geometry Model

A set of parameters is needed to define the missile inlet geometry so that a design space can be formed for the opti-

Table 1 Fixed parameters

No.	Parameter	Definition
1	D	Cowl diameter
2	r_f	Centerbody radius of constant cross-sectional region
3	x_g	Length of inlet for computation
4	x_l	Length of inlet for computation (=x_g)
5	x_n	Length of inlet for computation (=x_g)
6	r_m	External diameter

Table 2 Parameters to optimize

No.	Parameter	Definition
1	θ_1	Initial cone angle
2	θ_2	Final cone angle
3	x_d	Axial location of throat
4	r_d	Radial location of throat
5	x_e	Axial location of end of "constant" cross section
6	θ_3	Internal cowl lip angle
7	H_{ej}	Height at end of constant cross section
8	H_{fk}	Height at beginning of constant internal cross section

Note: All angles measured positive in counterclockwise direction.

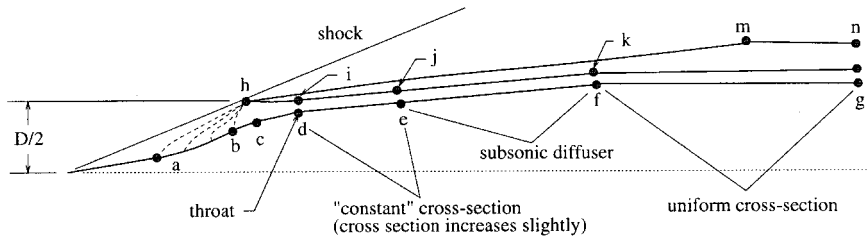

Fig. 1 Supersonic missile inlet geometry model.

mization. Figure 1 shows the model of the missile geometry, which is composed of six fixed parameters and eight design variables given in Tables 1 and 2, respectively. The missile inlet is axisymmetric and the coordinates are given in terms of axial x and radial r positions.

The external compression is achieved using an initial cone from the centerbody leading edge to point a followed by an isentropic compression ramp (a–b). The isentropic compression waves coalesce at the cowl lip, as does the conical shock from the centerbody leading edge. The internal compression starts at the entrance of the duct (c–h) and is followed by the curve on the centerbody (c–d) and the curve on the inner cowl (h–i). The connection between b and c is a straight line. The throat is located at (d–i) and has the minimum area in the duct. Following the throat is the near constant area throat section (d–e, i–j). The near constant area throat section has a slight divergence to compensate for the boundary layer that is growing. To obtain high total pressure recovery, the shock train must be able to be contained within this throat section. The subsonic diffuser further slows down the flow going into the transport duct (f–g). The transport duct has a constant cross-sectional area and transports the flow to the combustor with low flow energy loss. Upstream of the throat, the curves are required to have continuous slopes at the connections. The duct is composed of entirely straight lines downstream of the throat. The external cowl is formed by an ellipse that is considered to have low cowl wave drag[11] and has been not optimized in this study.

The inlet is required to start at Mach 2.6. The throat area is therefore computed to be able to swallow the normal shock at Mach 2.6 according to one-dimensional physics.[11,12] With the initial cone angle and final external turning, the isentropic compression turning is known and the curve shape (a–b) is computed using the method of characteristics. The curve c–d is made by an ellipse if possible. If no ellipse exists to fit c–d, a cubic line is used. The advantage of an ellipse curve over a cubic line is that the ellipse is monotonic for both coordinates and slope. The cubic line can have a deflection. The curve at the inner cowl lip h–i is a cubic. To ensure that the minimum cross section occurs at point i, a slope discontinuity is allowed at point i. Usually, such slope discontinuity is small and the results show that inlet performance benefits from this treatment.

If the radial position r_e is allowed to vary, the designed geometry can exhibit a slope discontinuity at location e–j. Because the analysis tool NIDA is based on one-dimensional smooth duct empirical correlation in this region, the results reported from NIDA would not be reliable for such geometries and may mislead the high-level accuracy analysis. We therefore only allow x_e to freely vary and require r_e to fall on the straight line between points d and f. Because NIDA computes the duct performance according to the cross-sectional area and wall divergent angle, this treatment will not reduce the design search space for the optimization. Because the total pressure of the inlet is the only object of the optimization at the current stage, the external cowl shape, and therefore, the cowl wave drag were kept unchanged. The external cowl shape was specified by UTRC (Ref. 13). The length of the inlet was also specified by UTRC.

All of the constraints are nonlinear inequality constraints and are continuous.[14] Except for the obvious geometry constraints such as $x_e > x_d$, $r_c > r_b$, the following constraints are required by aerodynamics and other disciplines:

1) The cross-sectional area at the throat must be the minimum within the whole duct from the entrance to the exit.

2) The angle between the inner and external cowl at the cowl lip should not be less than 3 deg for manufacturing purposes.

3) The minimum cowl wall thickness should not be less than 0.1 in., so that the cowl wall has sufficient strength.

4) The duct downstream of the throat must be monotonically divergent.

IV. Design Space Search

Figures 2 and 3 are two trade study results for an initial cone angle and throat axial location. The gaps in the curves represent points where NIDA did not yield a feasible solution, thus indicating that the design space determined by NIDA is nonsmooth. Therefore, if we were only to rely on the gradient-based optimum search procedure, it would likely converge to a nonglobal local optimum. We thus employed a GA optimizer[15] [Genetic Algorithm for Design Optimization (GADO)] and a multistart gradient line search optimizer CFSQP (Ref. 3). Both optimizers use RP to obtain the population and start points. CFSQP implements a quasi-Newton method to solve a nonlinear constrained optimization problem by fitting a sequence of quadratic programs.

V. Results and Discussion

Employing the aforementioned methodology, we started the design optimization from the original inlet design obtained using NIDA, but without any automated optimization. The de-

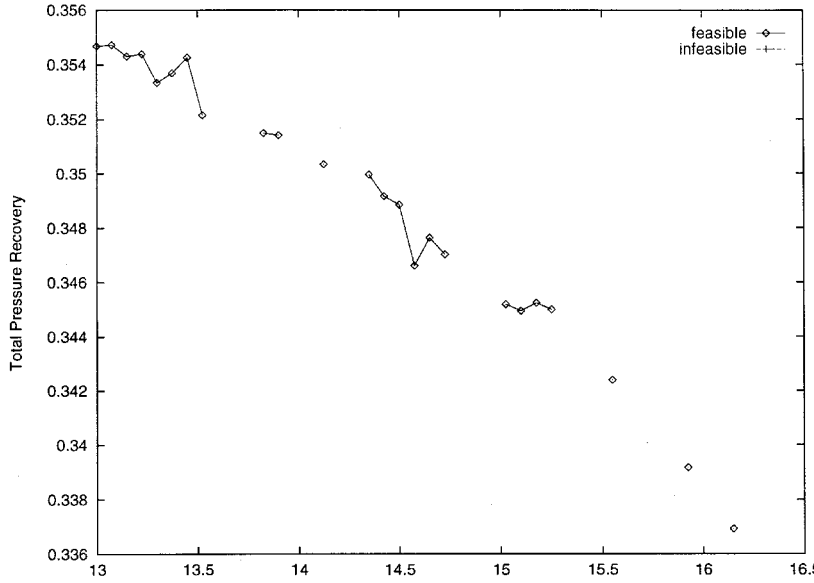

Fig. 2 Trade study of total pressure recovery vs the initial cone angle.

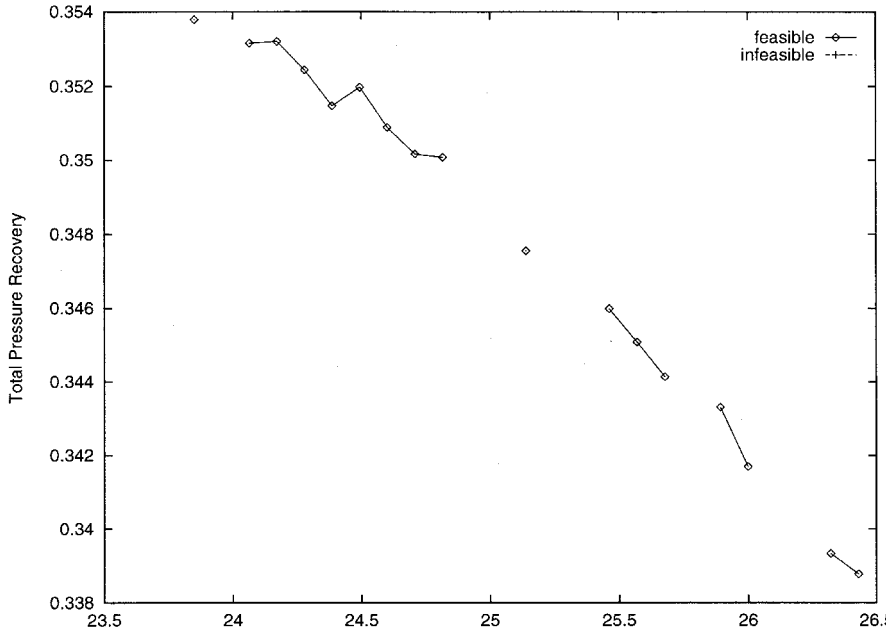

Fig. 3 Trade study of total pressure recovery vs the throat axial location.

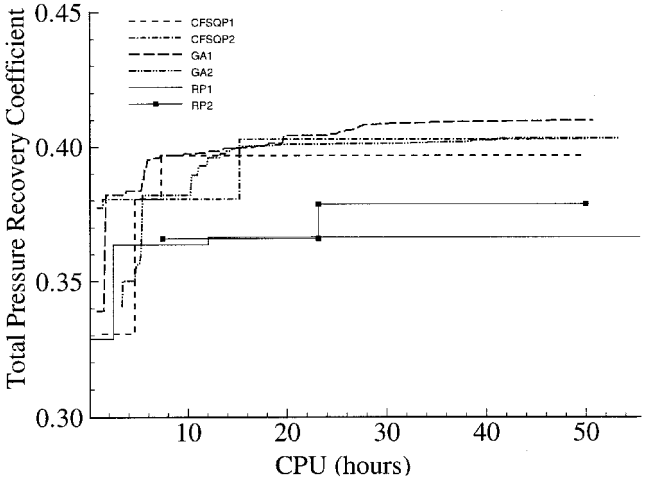

Fig. 4 Optimization history.

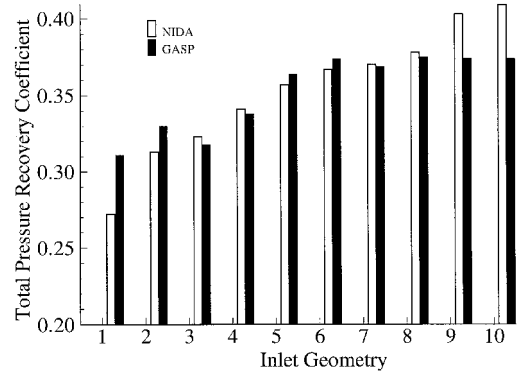

Fig. 5 Total pressure recovery comparison for inlet geometries obtained during the optimization procedure.

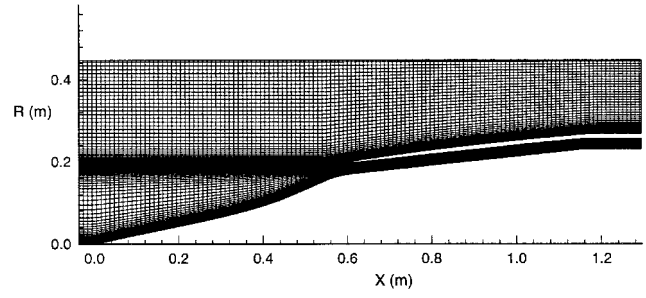

Fig. 6 Mesh for the flowfield computation of the missile inlet.

sign methodology was able to increase the total pressure recovery from the original value of 0.309 to 0.409, based on NIDA evaluation. This is a 32% increase and represents a very significant improvement. The limited number of GASP verifications reports a total pressure recovery optimum value of 0.375. The GASP result confirms an improvement in total pressure recovery compared with the original design, but the optimum value of GASP is 9% lower than that of NIDA.

Figure 4 is the optimization history with GA, multistart CFSQP, and RPs. Typically, a CPU time of 50 h on the DEC Alpha 2100 workstation is sufficient to obtain the optimum. GA and multistart CFSQP outperform the RP. GA has slightly higher optimum value than multistart CFSQP. This may be because the search range in a nonsmooth design space for CFSQP using line search is limited.

The basis for the multilevel design strategy is that the simple and sophisticated analysis should have similar trends. That is, when the simple analysis says one design is better than the other, the sophisticated analysis generally agrees. Such a trend is confirmed in Fig. 5 for a limited number of inlet geometries obtained during the optimization procedure. For most of the points, NIDA and GASP agree well, not only for ranking, but also for value. It is seen that when the the total pressure recovery value is higher than 0.375, NIDA continues to report a higher value up to 0.409 while GASP verification becomes flat. The disagreement may be because the optimizers reached the range where the empirical correlations in NIDA are invalid.

For those inlet geometries verified by GASP, Table 3 lists some important inlet performance parameters. The first three columns are plotted in Fig. 5. The relative weight flow W_R is defined as the ratio of the actual captured mass flow to the maximum captured mass flow, i.e., the mass flow in the freestream corresponding to the streamtube that intersects the cowl leading edge. The inlet distortion is obtained from

$$\text{Distortion} = (P_{r\max} - P_{r\min})/P_{r\text{mean}}$$

The geometry contraction ratio (CR) is

$$\text{CR} = (\text{Captured Area})/(\text{Throat Area})$$

Table 3 indicates that the design with a higher contraction ratio generally has the higher total pressure recovery. This agrees with inlet design principles. The contraction ratio was increased from 3.06 to 3.934 while maintaining the capability to start the inlet at Mach 2.6. All of the designs in Table 3 with a total pressure recovery higher than 0.341 and a lower recovery less than 0.378 based on NIDA evaluation have less than 3-deg slope discontinuities at the throat locations on the inner cowl surface. The discontinuity increases with the total pressure recovery value and reaches about 10 deg when the TPR is 0.409. If we did not relax the slope condition at the throat we would lose an important part of the design space. GASP computation did not show flow separation caused by this slope discontinuity. The exit distortion for all of the inlets is generally low.

The following is the Navier–Stokes flowfield analysis for the optimum case based on the optimal GASP evaluation, case 7. The computational domain is axisymmetric and composed of an inner and outer zone. Figure 6 is the center plane of the mesh used for this computation. The inner zone is from the centerbody leading edge through the internal channel to the exit of the inlet. The outer zone is the flowfield from the incoming freestream through the external surface of the cowl. Tables 4–8 summarize the geometry, flow, and mesh parameters for the computation. In Tables 4–8, δ_{in} is the boundary-layer thickness computed at the entrance of the inlet on the center body, and δ_{out} is the boundary-layer thickness computed at the streamwise midway location of the external cowl.

Table 3 Inlet performance for inlet geometries obtained during the optimization procedure

No.	$P_t/P_{t\infty}$ NIDA	$P_t/P_{t\infty}$ GASP	W_R	CR	Distortion
1	0.272	0.311	0.959	2.979	0.160
2	0.313	0.330	0.962	3.187	0.116
3	0.341	0.338	0.946	3.295	0.135
4	0.357	0.364	0.964	3.409	0.156
5	0.367	0.374	0.950	3.570	0.108
6	0.370	0.369	0.952	3.581	0.079
7	0.378	0.375	0.941	3.628	0.142
8	0.409	0.374	0.922	3.934	0.088
9	0.403	0.374	0.935	3.851	0.16

Table 4 Geometry parameters of inlet geometry 7

No.	Parameter	Value
Fixed		
1	D	0.381 m
2	r_f	0.231 m
3	x_f	1.158 m
4	x_m	1.158 m
5	x_n	1.158 m
6	r_m	0.269 m
Variable		
1	θ_1	12.00 deg
2	θ_2	24.00 deg
3	x_d	0.622 m
4	r_d	0.172 m
5	x_e	1.046 m
6	θ_3	1.16 deg
7	H_{ej}	0.027 m
8	H_{fk}	0.026 m

Table 5 Flow conditions

Parameter	Value
M_∞	4.0
$P_{t\infty}$	6.817×10^5
$T_{t\infty}$	914.76 K
Attack angle	0.0 deg
Reynolds number	5.959×10^6/m
δ_{in}	0.013 m
δ_{out}	0.0054 m

Table 6 Inner grid parameters

Parameter	Value
Grid point number in X	133
Grid point number in R	121
$\Delta x/\delta_{in}$	0.77
$\Delta r^+_{1\max,\text{centerbody}}$	7.4
$\Delta r^+_{1\text{av,centerbody}}$	2.4
$\Delta r^+_{1\max,\text{cowl}}$	3.5
$\Delta r^+_{1\text{av,cowl}}$	1.8

Table 7 Outer grid parameters

Parameter	Value
Grid point number in X	133
Grid point number in R	81
$\Delta x/\delta_{out}$	1.85
$\Delta r^+_{1\max}$	0.065
$\Delta r^+_{1\text{av}}$	0.0167

Table 8 Grid points within the boundary layers

Wall boundary layer	Number of grid points
Wall of the centerbody	57
Inner wall of the cowl	50
Inner wall of the cowl	40

At the inlet critical operating condition, the exit of the inlet is subsonic, and, therefore, the exit back pressure is a necessary boundary condition for the computation. A series of computations are needed to search the back pressure that yields the critical flow for the inlet. The critical back pressure tolerance is less than 1%, i.e., a 1% increase in the converged value for the back pressure will cause the inlet to unstart. The total pressure recovery calculated based on mass-weighted average, area-weighted average, and stream thrust-weighted average are, respectively,

$$P_t/P_{t\infty\,\text{mass average}} = \frac{1}{P_{t\infty}} \frac{\int \rho u P_t \, ds}{\int \rho u \, ds} = 0.3748$$

$$P_t/P_{t\infty\,\text{area average}} = \frac{1}{Pt_\infty} \frac{\int P_t \, ds}{\int ds} = 0.3741$$

$$P_t/P_{t\infty\,\text{stream thrust}} = \frac{1}{Pt_\infty} \frac{\int (\rho u^2 + p) P_t \, ds}{\int (\rho u^2 + p) \, ds} = 0.3740$$

where s is the area in radial direction of the axisymmetric computational domain.

Figure 7 shows the Mach number contours of the flowfield. The oblique shock wave and isentropic compression waves generally focus around the leading edge of the cowl as intended. The details of the Mach number contours in the throat area are shown in Fig. 8. There is a shock generated by the cowl leading edge that intersects the centerbody. The cowl shock does not cause separation on the centerbody. The reflecting shock from the centerbody intersects with another oblique shock wave from the cowl surface and forms a supersonic tongue downstream of the intersection. The light blue sonic line shows that the flow after the oblique shock wave intersection gradually becomes subsonic. This maintains a high total pressure for the flow in that region. Figure 9 shows the total pressure contours and demonstrates that the gradual change of the supersonic to subsonic flows benefits the total pressure loss with a region shown by the color green, whereas the flow separations induced by the shock wave/turbulent boundary-layer interaction cause serious total pressure loss. The low energy flow from the separation strongly mixes with the main flow as a result of the turbulence and makes the downstream total pressure field uniform. This is desirable to reduce the distortion of the flow going into the combustor. The turbulent intensity is also enhanced by the terminal shock wave/turbulent boundary-layer interaction and reaches the maximum in the separation region (not shown).

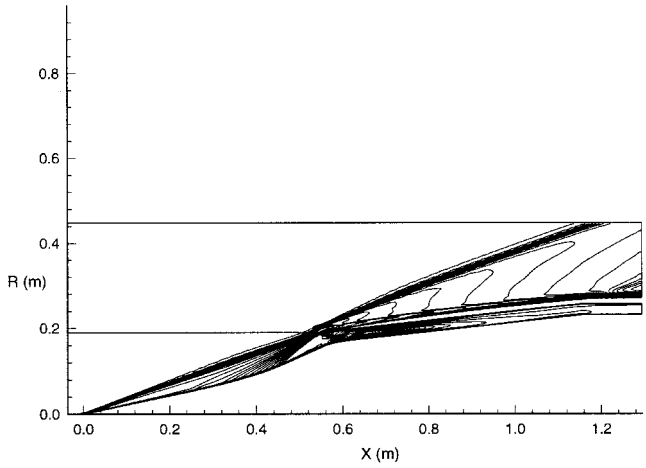

Fig. 7 Mach number contours of the inlet flowfield for inlet geometry 7.

Figure 10 displays the flow separations induced by the shock wave/turbulent boundary-layer interaction for different inlet geometries with increasing total pressure recovery. They are case 2 (Fig. 10a), case 4 (Fig. 10b), case 6 (Fig. 10c), and the optimum case 7 (Fig. 10d), respectively, in Table 3. Because the channels have mild divergence, these separation regions are necessary to form the second throat and support the strong compression wave (the intersection of the two oblique shocks) compressing the supersonic flow to subsonic. Figure 10 clearly shows the geometry evolution with the optimization. In most

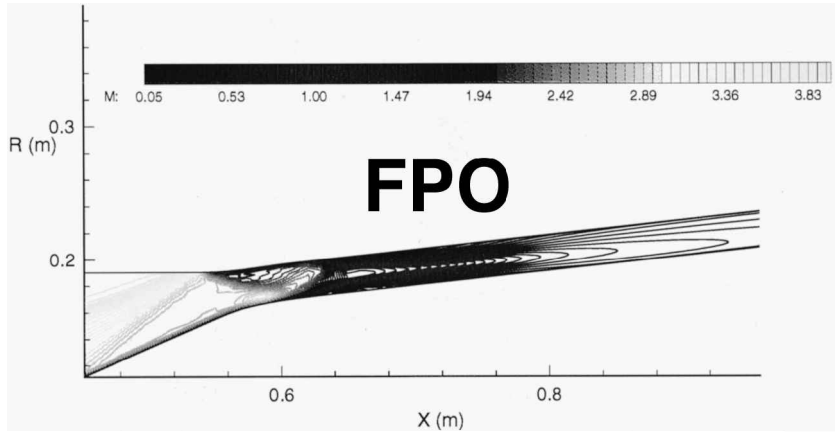

Fig. 8 Mach number contours of the inlet geometry 7 flowfield in the throat area.

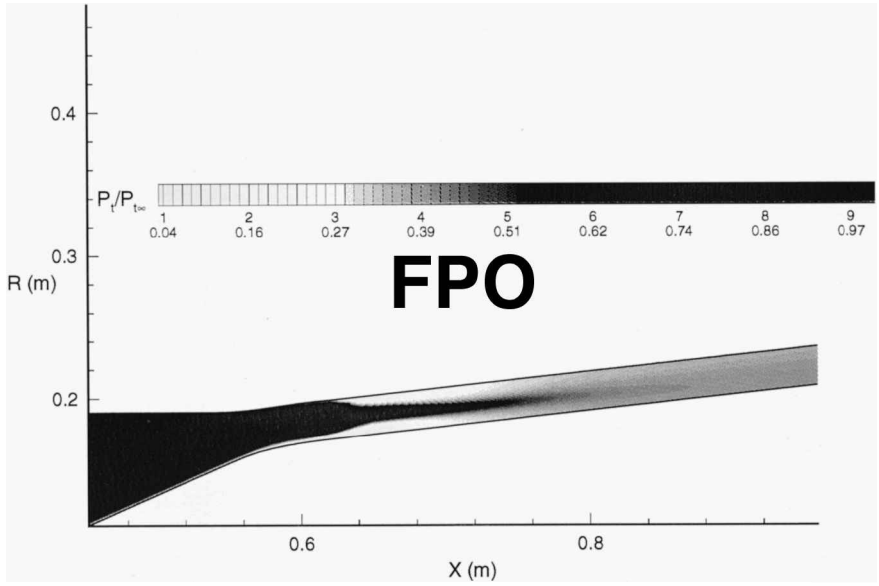

Fig. 9 Total pressure contours of the inlet geometry 7 flowfield in the throat area.

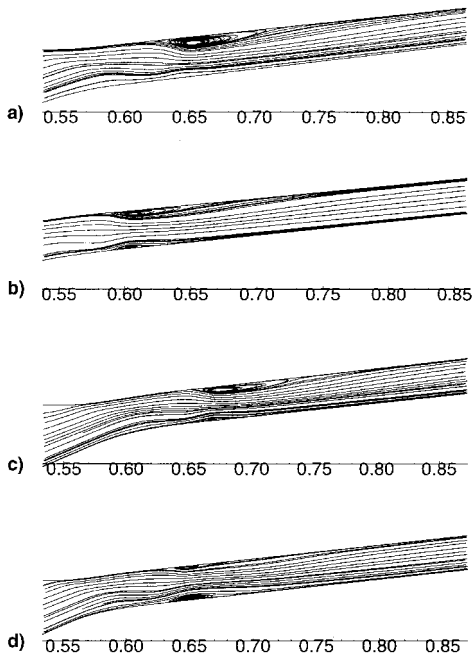

Fig. 10 Streamlines of the inlet flowfields in the throat area. Inlet geometry a) 2, b) 4, c) 6, and d) 7.

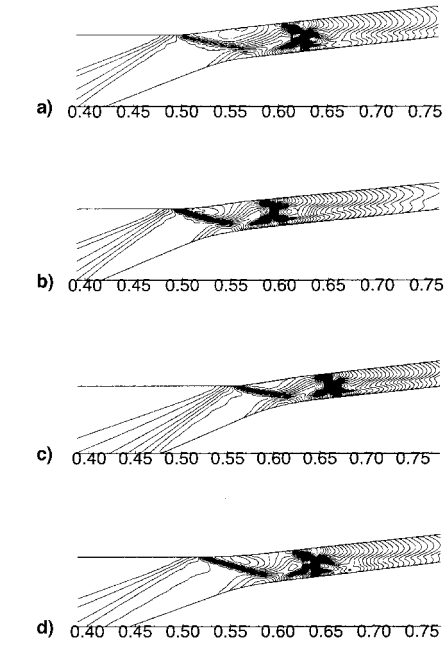

Fig. 11 Pressure contours of the inlet flowfields in the throat area. Inlet geometry a) 2, b) 4, c) 6, and d) 7.

cases, there is a large separation on the inner cowl surface and a small separation on the centerbody surface. The optimum case has the smallest separation region and throat area, with a larger separation on the centerbody than on the inner cowl surface. The flow separation is mainly determined by the shock wave intensity. Figure 11 presents the pressure contours of the flowfield in the throat region and shows the shock wave systems inside the inlets. The optimum case has weak intensity of the terminal shock train because it has a high contraction ratio and a low throat Mach number.

In Table 3, it is evident that the relative weight flow is typically 0.95. Theoretically, the relative weight flow should be 1.0 if the shock wave focuses on the cowl lip as the design requires. The reasons for this difference are as follows:

1) NIDA uses a two-dimensional aerodynamics model to determine the wave focus point without taking into account the boundary-layer effect. When the flowfield is computed using the GASP Navier–Stokes solver, the pressure after the oblique shock from the centerbody leading will be slightly increased because of the centerbody boundary-layer displacement. The shock and isentropic compression waves are therefore slightly pushed away and some flow is spilled.

2) Even if the oblique shock wave from the centerbody leading edge intersects the cowl lip, the numerical diffusion broadens the shock wave at the cowl lip and makes the shock wave look like a strong compression wave, which will also result in some flow spillage around the cowl lip. The diffused shock wave at the cowl lip can be seen from Figs. 7, 8, and 11. Such shock wave diffusion may be reduced by aligning the mesh with the shock wave and mesh adaptation.

It is noted that inlet geometries 5, 7, and 8 have nearly the same total pressure recovery evaluated by GASP but quite different geometries. Table 9 presents the geometry variables for cases 5 and 8. Figure 12 shows the total pressure recovery variation along the inlet axial axis for these three inlet geometries. Inlet geometries 5 and 7 have more internal compression compared to inlet geometry 8.

Inlet geometries 5 and 7 have different inner cowl lip angles and throat locations. The duct divergence after the throat is also quite different. Inlet geometry 7 has the stronger cowl lip shock loss because it has a smaller inner cowl angle than inlet geometry 5 (Fig. 11). The Mach number before the terminal shock for inlet geometry 7 is smaller than that of inlet geometry 5 because of its higher contraction ratio, and thus, the terminal shock intensity of inlet geometry 7 is weaker (see Figs. 10 and 11). Therefore, inlet geometry 7 has a smaller total pressure loss because of the terminal shock wave/turbulent boundary-layer interaction. However, after the terminal shock, inlet geometry 7 has a stronger pressure gradient and more rapidly turbulent boundary-layer development, resulting in a larger total pressure loss. Table 3 shows that inlet geometry 5 has a lower distortion than inlet geometry 7.

The final external turning angle of inlet geometry 8 is significantly larger than those of inlet geometries 5 and 7. The supersonic flow is largely externally compressed with a nearly normal shock located at the cowl lip. The total pressure drops sharply as a result of the strong cowl lip shock and the boundary-layer separation induced by the shock. Because of the highest contraction ratio and closer throat location to the cowl leading edge, the flow downstream of the cowl lip shock is weakly supersonic and goes to subsonic quickly.

Comparison of inlet geometries 5, 7, and 8 means that, for a supersonic inlet, the same total pressure recovery may be

Table 9 Geometry variables of inlet geometries 5 and 8

No.	Parameter	Value
Inlet geometry 5		
1	θ_1	11.40 deg
2	θ_2	23.49 deg
3	x_d	0.64 m
4	r_d	0.176 m
5	x_e	1.064 m
6	θ_3	5.83 deg
7	H_{ej}	0.030 m
8	H_{fk}	0.0292 m
Inlet geometry 8		
1	θ_1	12.73 deg
2	θ_2	26.20 deg
3	x_d	0.60 m
4	r_d	0.170 m
5	x_e	1.087 m
6	θ_3	3.89 deg
7	H_{ej}	0.024 m
8	H_{fk}	0.032 m

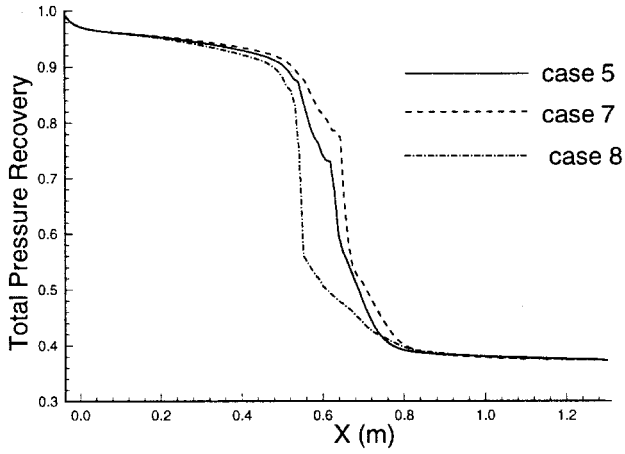

Fig. 12 Total pressure recovery distribution along the axis.

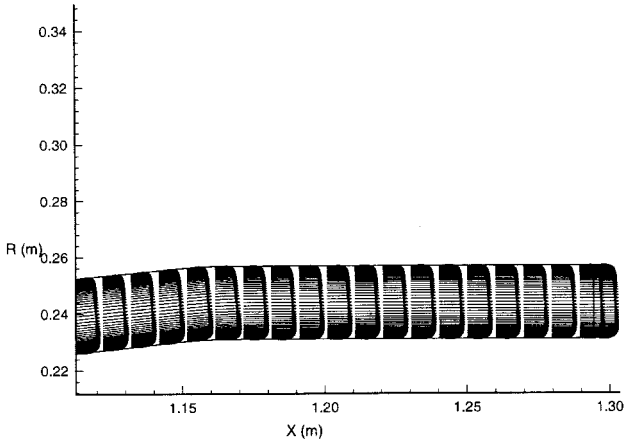

Fig. 13 Velocity profiles in the region of the exit for inlet geometry 7.

obtained by controlling different geometry parameters. This would make the design more difficult if we did not have an automated optimization procedure.

Figure 13 is the velocity profiles of inlet geometry 7 in the region of the inlet exit. The flow is shown to be quite uniform.

VI. Flowfield Computation

The flowfield computation using GASP starts with the supercritical flow that is supersonic from the entrance to the exit. When a back pressure is imposed at the exit, a terminal shock appears with this separation region. The process to reach the steady state is the motion process of this shock-separation (SS) system. When the back pressure is substantially higher than the critical back pressure, the propagation speed of the SS system is fast and the shock is quickly pushed out of the entrance as subcritical flow.[13] When the back pressure is approaching the critical value, the propagation speed of the SS system is very slow. This makes the computation particularly CPU time intensive. When a critical flow is considered to be obtained, the solution will be run again for another substantially long time to check if the SS system is displaced. This will tell if the SS system is still slowly moving or finally stable. Using the GASP code, typically 24 hours of CPU time is needed to achieve a converged flowfield on a DEC Alpha 2100 workstation computer. It needs about 5 days to search the back pressure value for the critical flow with a tolerance of 1%.

Mesh refinement tests were conducted. The number of mesh points in the radial direction were doubled. In the axial direction, the mesh spacing was halved from the cowl leading edge to downstream of the shock/boundary-layer interaction region. The variation in total pressure recovery caused by mesh refinement is less than 1%, which is consistent with our TPR accuracy tolerance. The mesh refinement tests confirm that the mesh resolution used for the GASP verifications is sufficient.

The design quantities we have obtained so far are still at the theoretical stage. The final design needs to be confirmed by the experiment.

VII. Conclusions

A multilevel design strategy for a supersonic missile inlet design was developed. The multilevel design strategy combines an efficient simple physical model analysis tool and a sophisticated CFD Navier–Stokes analysis tool. The efficient simple analysis tool is incorporated into the optimization loop and the CFD Navier–Stokes analysis tool is used to verify, select, and filter the final design. GA and multistart gradient line search optimizers are used to search the nonsmooth design space. A geometry model for the supersonic missile inlet is developed. The simple and sophisticated analysis tools generally have the same trend to evaluate the measure of merit.

A supersonic mixed compression missile inlet with fixed geometry and no bleed was designed using the multilevel design strategy. The inlet starts at Mach 2.6 and cruises at Mach 4. The inlet total pressure recovery of 0.409 has been obtained, which represents an improvement of 32% based on the NIDA evaluation using a two-dimensional aerodynamic model and one-dimensional empirical correlations. Verifications using the Navier–Stokes solver of GASP report a 9% lower optimum value than that of NIDA but, nonetheless, showed a significant improvement in performance (23%) compared to the initial design. A detailed flowfield analysis is presented and shows that the main total pressure loss occurs in the region of the cowl lip shock, terminal shock, and in the region downstream of the separation induced by the terminal shock wave/turbulent boundary-layer interaction because of the spread of the low flow energy and turbulent boundary-layer development.

Acknowledgments

This research is part of the Hypercomputing and Design (HPCD) project based at Rutgers University. The HPCD project is supported by the Advanced Research Projects Agency of the Department of Defense through Contract ARPA-DABT 63-93-C-0064, monitored by Bob Lucas. UTRC supported the efforts of Martin Haas under its IR&D program. We appreciate the helpful discussions with David Sobel at United Technologies Research Center, and Madara Ogot at the Department of Mechanical and Aerospace Engineering, Rutgers University. The contents of this paper do not necessarily reflect the position of the United States government and official endorsement should not be inferred.

References

[1]Gelsey, A., Knight, D., Gao, S., and Schwabacher, M., "NPARC Simulation and Redesign of the NASA P2 Hypersonic Inlet," AIAA Paper 95-2760, July 1995.

[2]Shukla, V., Gelsey, A., Schwabacher, M., Smith, D., and Knight, D., "Automated Redesign of the NASA P2 Hypersonic Inlet Using Numerical Optimization," 32nd Joint Propulsion Conf., Lake Buena Vista, CA, July 1996.

[3]Lawrence, C., Zhou, J., and Tits, A., "Users Guide for CFSQP Version 2.3: AC Code for Solving (Large Scale) Constrained Nonlinear (Minimax) Optimization Problems, Generating Iterates Satisfying All Inequality Constraints," Inst. for Systems Research, Univ. of Maryland, TR 94-16rl, College Park, MD, Nov. 1994.

[4]Jou, W., Huffman, W., Young, D., Melvin, R., Bieterman, M., Hilmes, C., and Johnson, F., "Practical Consideration in Aerodynamic Design Optimization," *Proceedings of the 12th AIAA Computational Fluid Mechanics Conference* (San Diego, CA), AIAA, Washington, DC, 1995, pp. 950–960.

[5]Jameson, A., "Aerodynamic Design via Control Theory," *Journal of Scientific Computing*, Vol. 3, 1988, pp. 233–260.

[6]Jameson, A., "Optimum Aerodynamic Design Using CFD and

Control Theory," *Proceedings of the 12th AIAA Computational Fluid Mechanics Conference* (San Diego, CA), AIAA, Washington, DC, 1995, pp. 926–949.

[7]Yamamoto, K., and Inoue, O., "Application of Genetic Algorithm to Aerodynamic Shape Optimization," *Proceedings of the 12th AIAA Computational Fluid Mechanics Conference* (San Diego, CA), AIAA, Washington, DC, 1995, pp. 43–51.

[8]Dervieux, A., Male, J.-M., and Marco, N., "Numerical vs. Non-Numerical Robust Optimisers for Aerodynamic Design Using Transonic Finite-Element Solvers," *Proceedings of the 12th AIAA Computational Fluid Mechanics Conference* (San Diego, CA), AIAA, Washington, DC, 1995, pp. 1339–1347.

[9]Aly, S., Marconi, F., Ogot, M., Pelz, R., and Siclari, M., "Stochastic Optimization Applied to CFD Shape Design," *Proceedings of the 12th AIAA Computational Fluid Mechanics Conference* (San Diego, CA), AIAA, Washington, DC, 1995, pp. 11–20.

[10]Ogot, M., and Alag, S., "An Effective Mixed Annealing/Heuristic Algorithm for Kinematic Mechanical Design," *Journal of Mechanical Design*, Vol. 117, 1995, pp. 409–418.

[11]Haas, M., Elmquist, R., and Sobel, D., "NAWC Inlet Design and Analysis (NIDA) Code, Final Report," United Technologies Research Center, Rept. R92-970037-1, 1992.

[12]Seddon, J., and Goldsmith, E., *Intake Aerodynamics*, AIAA, New York, 1985.

[13]Zha, G.-C., "Flow Field Analysis of the Baseline Cheapshot Missile Inlet Using a Navier-Stokes Solver," Dept. of Mechanical and Aerospace Engineering, Rutgers Univ., ARPA Inlet Design Group, Rept. 5, Piscataway, NJ, Sept. 1995.

[14]Gelsey, A., Schwabacher, M., and Smith, D., "Using Modeling Knowledge to Guide Design Space Search," *Artificial Intelligence in Design '96*, 4th International Conference on Artificial Intelligence in Design (Stanford Univ., Stanford, CA), Kluwer Academic, Norwell, MA, 1996, pp. 367–385.

[15]Rasheed, K., Hirsh, H., and Gelsey, A., "A Genetic Algorithm for Continuous Design Space Search," *Artificial Intelligence in Engineering*, Vol. 11, No. 3, 1997, pp. 295–305.